Available online at www.sciencedirect.com
SCIENCE DIRECT®
Journal of Contaminant Hydrology 61 (2003) 157–174
JOURNAL OF Contaminant Hydrology
www.elsevier.com/locate/jconhyd

Solute transport in crystalline rocks at Äspö — I: Geological basis and model calibration

Martin Mazurek [a,*], Andreas Jakob [b], Paul Bossart [c]

[a] *Rock-Water Interaction Group (RWI), Institute of Geological Sciences, University of Bern, Baltzerstr. 1, CH-3012, Bern, Switzerland*
[b] *Waste Management Laboratory LES, Paul Scherrer Institute, Villigen-PSI, Switzerland*
[c] *Geotechnical Institute, Bern, Switzerland*

Received 29 August 2001; received in revised form 28 January 2002; accepted 11 April 2002

Abstract

Water-conducting faults and fractures were studied in the granite-hosted Äspö Hard Rock Laboratory (SE Sweden). On a scale of decametres and larger, steeply dipping faults dominate and contain a variety of different fault rocks (mylonites, cataclasites, fault gouges). On a smaller scale, somewhat less regular fracture patterns were found. Conceptual models of the fault and fracture geometries and of the properties of rock types adjacent to fractures were derived and used as input for the modelling of in situ dipole tracer tests that were conducted in the framework of the Tracer Retention Understanding Experiment (TRUE-1) on a scale of metres. After the identification of all relevant transport and retardation processes, blind predictions of the breakthroughs of conservative to moderately sorbing tracers were calculated and then compared with the experimental data. This paper provides the geological basis and model calibration, while the predictive and inverse modelling work is the topic of the companion paper [J. Contam. Hydrol. 61 (2003) 175].

The TRUE-1 experimental volume is highly fractured and contains the same types of fault rocks and alterations as on the decametric scale. The experimental flow field was modelled on the basis of a 2D-streamtube formalism with an underlying homogeneous and isotropic transmissivity field. Tracer transport was modelled using the dual porosity medium approach, which is linked to the flow model by the flow porosity. Given the substantial pumping rates in the extraction borehole, the transport domain has a maximum width of a few centimetres only. It is concluded that both the uncertainty with regard to the length of individual fractures and the detailed geometry of the network along the flowpath between injection and extraction boreholes are not critical because flow is largely one-dimensional, whether through a single fracture or a network. Process identification and model calibration were based on a single uranine breakthrough (test PDT3), which clearly showed that matrix diffusion had to be included in the model even over the short experimental time scales,

* Corresponding author. Tel.: +41-31-631-8781; fax: +41-31-631-4843.
E-mail address: mazurek@geo.unibe.ch (M. Mazurek).

PII: S0169-7722(02)00137-7

evidenced by a characteristic shape of the trailing edge of the breakthrough curve. Using the geological information and therefore considering limited matrix diffusion into a thin fault gouge horizon resulted in a good fit to the experiment. On the other hand, fresh granite was found not to interact noticeably with the tracers over the time scales of the experiments.

While fracture-filling gouge materials are very efficient in retarding tracers over short periods of time (hours–days), their volume is very small and, with time progressing, retardation will be dominated by altered wall rock and, finally, by fresh granite. In such rocks, both porosity (and therefore the effective diffusion coefficient) and sorption K_ds are more than one order of magnitude smaller compared to fault gouge, thus indicating that long-term retardation is expected to occur but to be less pronounced.

Keywords: Fractured rock; Fault geometry; Fault gouge; Matrix diffusion; Dipole tracer experiments; Transport modelling

1. Introduction

In the framework of the Fracture Characterisation and Classification Project (Mazurek et al., 1996; Bossart et al., 2001), the geological and hydraulic properties of faults and fractures of different sizes were studied in the Äspö Hard Rock Laboratory in SE Sweden. The laboratory is located in granitic rocks at depths of 0–450 m below surface (general overview in Stanfors et al., 1997, 1999). One of the motivations for these investigations was to support the quantitative evaluation of dipole tracer tests that were conducted in the framework of the Tracer Retention Understanding Experiment (TRUE-1, Winberg, 1996; Winberg et al., 2000). The understanding of the mechanistic principles of the faulting process, together with a detailed characterisation of the hydrothermal water/rock interactions experienced by the rocks, are important for the description of the geometry of the fracture network on all scales, as well as for the characterisation of the geochemical properties of the rocks that interact with the tracers during the experiments.

TRUE-1 consists of a number of in situ hydraulic and tracer tests conducted on a scale of metres, using conservative, weakly and moderately sorbing radioactive tracers. These experiments were accompanied by a modelling exercise where eight teams were asked to blindly predict the breakthrough curves for a number of tracers with different geochemical behaviours. Different conceptual models were applied by different teams, including discrete fracture networks, channel networks, stochastic continuum and a streamtube/double-porosity approach. The results and the evaluation of this exercise are provided by Elert and Svensson (2001), and we restrict ourselves to the presentation of our own contribution.

This paper defines the geological basis for the model calculations by means of a structural and petrological analysis of fractures on a wide range of scales. Conceptual models of fracture geometries, distributions of rock types and rock properties relevant for tracer/rock interactions (e.g. matrix diffusion, sorption) are derived. The analysis of a uranine breakthrough curve (test PDT3) that was provided as input to the modelling teams is used for the identification of relevant processes that affect tracer transport. Together with

the geological information, rock domains in which tracer/rock interaction occurs over the experimental time scales are identified, and this finally allows the calibration of the transport model and subsequent predictive calculations of breakthrough curves. The results of the blind predictions, augmented by a refinement of the model by inverse modelling, are presented in the follow-up paper (Jakob et al., 2003).

The specific objectives of this paper include:

- the development of strategies on how "hard" and "soft" geological field data from a heterogeneous geological system can be simplified and used to constrain conceptual models that are needed for quantitative predictions of tracer transport in the dipole experiments,
- the identification of the relevant transport and retardation processes that govern tracer migration during the short-duration tracer experiments (in specific, the role of matrix diffusion),
- the identification of the rock domains in and around fractures in which these processes occur, and
- the extrapolation of the results to tracer transport through fractured granitic rock to larger scales in space and time.

2. Geological characterisation of decametric water-conducting features

A number of regional water-conducting faults that extend over kilometres were penetrated by the 3700 m long tunnel system (Stanfors et al., 1999; Rhén and Forsmark, 2000). By number, the largest part of visible water inflows into the tunnel is related to faults extending over distances in the decametre scale, and these are the focus of this section. Even smaller hierarchies of water-conducting fractures (metre-scale) are identified in boreholes, even though, in general, their transmissivity is lower and so they do not visibly discharge into the tunnel. These fractures are discussed below in Section 3.

2.1. Fault geometries

Close to 100 decametric water-conducting features, i.e. those that crosscut the entire tunnel profile and visibly discharge water into the tunnel, were studied and mapped (details in Mazurek et al., 1996). The analysis indicates that they are mostly related to steeply dipping faults. While flat-lying structures (fractures, joints) also exist in the tunnel, their sizes are more limited, and their transmissivities are in general not sufficient to result in water inflow points. The spacing of the water-conducting faults is ca. 10–20 m along tunnel, and transmissivities are typically 10^{-6}–10^{-4} m^2/s. Based on their geometry, five different types can be distinguished and are shown in Fig. 1. Each of these types of faults consists of two different elements, namely:

1) *master faults* along which shear displacement occurred and which are often associated with cohesive or incohesive fault rocks (such as cataclasites, fault breccias or gouges, see below), and

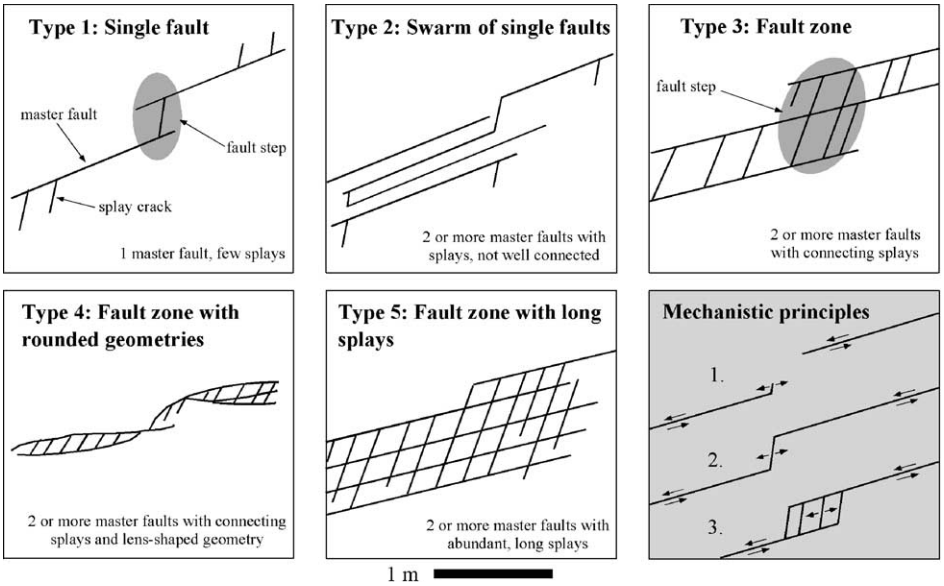

Fig. 1. Fault geometries of five types of water-conducting features on a scale of metres. The sketch in the lower right corner schematically illustrates the evolution of the growth and linkage of master faults and splay cracks, resulting in fault steps and locally different fault geometries.

2) *splay cracks* that are tensile structures (joints) and typically have an angle of ca. 20–60° to the master faults. Because no shear displacement occurred along these, they are in general devoid of fault rocks.

Fig. 1 shows that the geometric variability of the faults is substantial, ranging from simple structures such as single faults with only few splays (type 1) to highly complex networks consisting of several parallel master faults connected by splay cracks (e.g. type 5). The strike direction of all faults is predominantly NW–SE, and there is no discrimination among different fault types with respect to orientation. During fault growth, adjacent master faults may link together via splay cracks, which results in fault steps which consist of interconnected arrays of master faults and splay cracks (Fig. 1, bottom right). The observed fault geometries are consistent with the mechanistic principles of fault nucleation, propagation and linkage derived by Martel and Pollard (1989). Along strike, the fault anatomy is heterogeneous and includes geometrically simple segments (types 1 and 2 in Fig. 1) alternating with segments of more complex geometries, which contain several master faults connected by densely spaced splay cracks (e.g. in complex fault steps, types 3–5 in Fig. 1). The length of simple and complex segments within the faults lies in the order of metres to few tens of metres according to surface investigations of large outcrops. Thus, the geometric patterns of faults shown in Fig. 1 characterise the variability along strike of the faults rather than fundamentally different families of faults.

2.2. Fault rocks

Many of the faults described above clearly document recurrent events of deformation and related hydrothermal alteration/cementation. At least three major deformation styles and types of fault rocks can be distinguished:

1) *Mylonites*. Ductile deformation at elevated temperature (>400 °C), leading to locally foliated to mylonitic zones in the otherwise massive granites. Due to dynamic recrystallisation (which is inherent in the definition of a mylonite), no discrete fractures developed, and so mylonite zones per se are hydraulically no preferential flowpaths today. Due to recrystallisation of the fabric and the reduction of grain size, matrix porosity of mylonite is even lower than that of undeformed granite.
2) *Cataclasites*. A first stage of brittle deformation at elevated temperature led to brittle faulting and the development of fault breccias and gouges in the central parts of the faults. The deformation was followed by hydrothermal activity, leading to a partial cementation of the fault rocks (mainly by epidote, quartz and chlorite) and an alteration of the wall rocks. Cementation restored the cohesion of the fault rocks, thus resulting in cataclasites. There are indications that such events of faulting, followed by hydrothermal water/rock interactions, occurred recurrently throughout the long history of the Precambrian granites.
3) *Fault breccias and gouges*. Some of the younger stages of faulting were no longer related to events of hydrothermal water/rock interaction, such that brittle fault rocks that resulted from the shearing process remain as incohesive fault breccias and gouges today. Incohesive rocks have been observed in most of the investigated faults.

Faults observed today in the Äspö laboratory contain the integrated record of deformation and alteration events that affected the rocks over the last 2 Ga. Because older structures represent pre-existing mechanical heterogeneities for younger deformation events, the same structures were reactivated recurrently and so contain different types of fault rocks. Thus, the lithological heterogeneity is substantial within faults, and mylonites, cataclasites, fault breccias/gouges and wall rocks in various stages of hydrothermal alteration may occur along any single profile across a fault. The different rock units have highly contrasting properties, and relevant parameters such as porosity and sorption capacity may vary over orders of magnitude.

2.3. Detailed-scale anatomy of master faults

Dedicated large-diameter boreholes (ca. 1 m long, 25 cm in diameter) were drilled for the characterisation of the anatomy of master faults on a detailed scale. In order to minimise core damage, the drilling axis was chosen parallel to the fault strike, with the master fault centered in the core. In the laboratory, the recovered cores were first evacuated and then impregnated by fluorescent resin under a pressure of 10 bar. Rock slices and thin sections were prepared and used for the characterisation of the detailed geometries of rock types and pore spaces.

Fig. 2 (top part) shows the distribution of different rock units and of fractures in a profile across the fault plane. The fault was active during different deformation events and

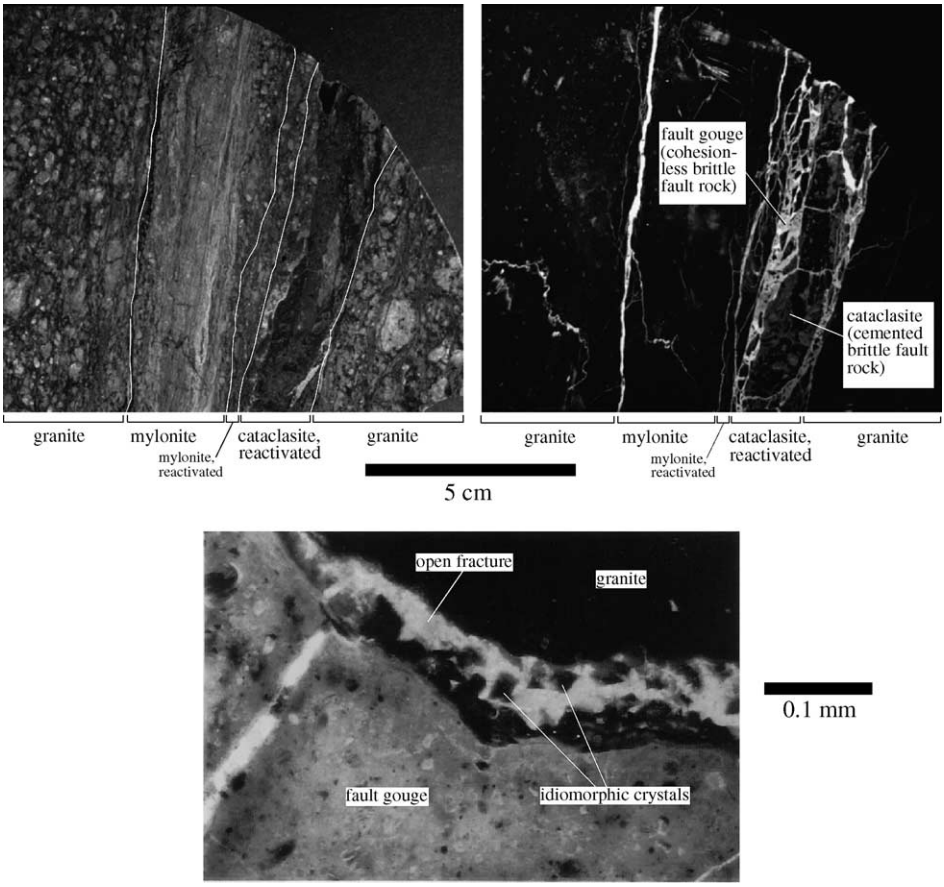

Fig. 2. Small-scale architecture of decametric faults. Top: structural elements recording recurrent activity (mylonite/cataclasite/fault gouge), shown in photos under visible light (left) and UV light (right, highlighting porosity). Bottom: interface between fault gouge and granitic wall rock observed in an impregnated thin section (UV light), showing a naturally open microfracture with idiomorphic crystals.

contains a variety of different fault rocks, ranging from mylonites to cataclasites and incohesive fault gouges. It can be seen that most of the open fractures through which flow may occur are located along the contacts of different rock types, in particular, along cataclasite and fault gouge horizons.

On a microscopic scale (Fig. 2, bottom), it is seen that the bulk mass of the fault gouge is highly porous but discrete open fractures are located along the contact to the wall rock. Flow may occur at the interface of fault gouge and wall rock, while the highly porous gouge material is accessible to diffusion. The fact that the fracture contains small idiomorphic crystals provides clear evidence that it is of natural origin and not due to sampling artifacts. On the basis of the impregnated thin sections, fault gouge porosity can be roughly estimated at 10–30 vol.%, whereas direct measurements are not available (and would be difficult to obtain).

It is obvious from Fig. 2 that the rock types adjacent to the actual flowpaths are mostly fault rocks (fault breccia/gouge, cataclasite, mylonite) and not granite. Over typical time scales of dipole experiments (hours–days), tracers are likely to interact with the immediate surroundings of the fractures. Due to their enhanced porosity and higher sorption capacity due to the presence of clay minerals, the dominant interaction is most probably with fault gouge and cataclasite. While granite constitutes the largest part of the bulk rock volume, its role for water/rock interaction during tracer tests is expected to be very limited.

3. Characterisation of smaller-scale fractures in the TRUE-1 block (length range of decimetres–metres)

3.1. Geometric and hydraulic properties of the fracture network

The so-called "TRUE-1 block" has been chosen as the target volume for dipole tracer testing because it is devoid of conductive, decametre-scale faults as the ones described above (these structures actually bound the block). The ca. 50 m long tunnel section through the TRUE-1 block at 400 m below surface is entirely free of visible water discharges or moisture zones. However, tunnel mapping and borehole evidence clearly indicate that it contains a network of smaller-scale fractures and faults with trace lengths in the range of decimetres to metres. Fracture patterns and orientations are less regular than on the larger scale, and a mechanistic explanation is less straightforward. Most likely, the fracture pattern was determined by the local stress field generated by movements along the larger faults that bound the block.

A series of boreholes was drilled through the TRUE-1 block, and their positions are shown in Fig. 3. Transmissivities were calculated from single-packer tests (measurement of differential outflow) and relate to intervals of 0.5 m length along hole. Sixty-five percent of all intervals have a transmissivity above the detection limit (ca. 10^{-10} m^2/s), with a maximum value of 2×10^{-6} m^2/s (Winberg, 1996). Thus, in spite of the absence of large faults, the whole TRUE-1 block is characterised by a very dense network of water-conducting features. In some of the boreholes, a positive correlation with fracture frequency can be identified.

Decametric faults, as described above, often reactivate pre-existing zones affected by ductile deformation. Schistose sections and mylonites also occur within the TRUE-1 block, accounting for 16% of the total core material. Borehole-wall imaging indicates that the average fracture frequency in mylonitic zones is around 7 m^{-1}, which is substantially higher than the overall average of 4 m^{-1}. Thus, similar to the larger scale, mylonites tend to focus and concentrate brittle fracturing. Moreover, fractures along pre-existing mylonites tend to be longer than fractures outside mylonitic zones (whose trace lengths are mostly below 1 m). On the basis of structural evidence, it is concluded that mylonites are potential zones of enhanced fracture connectivity.

While no clear distinction of interval transmissivities in and outside mylonites exists, hydraulic interference testing (Winberg, 1996) indicates that crosshole responses are specifically high within the most prominent mylonite zone penetrated by the boreholes. This zone is 1–2 m thick and can be identified in all boreholes. The large part of this zone

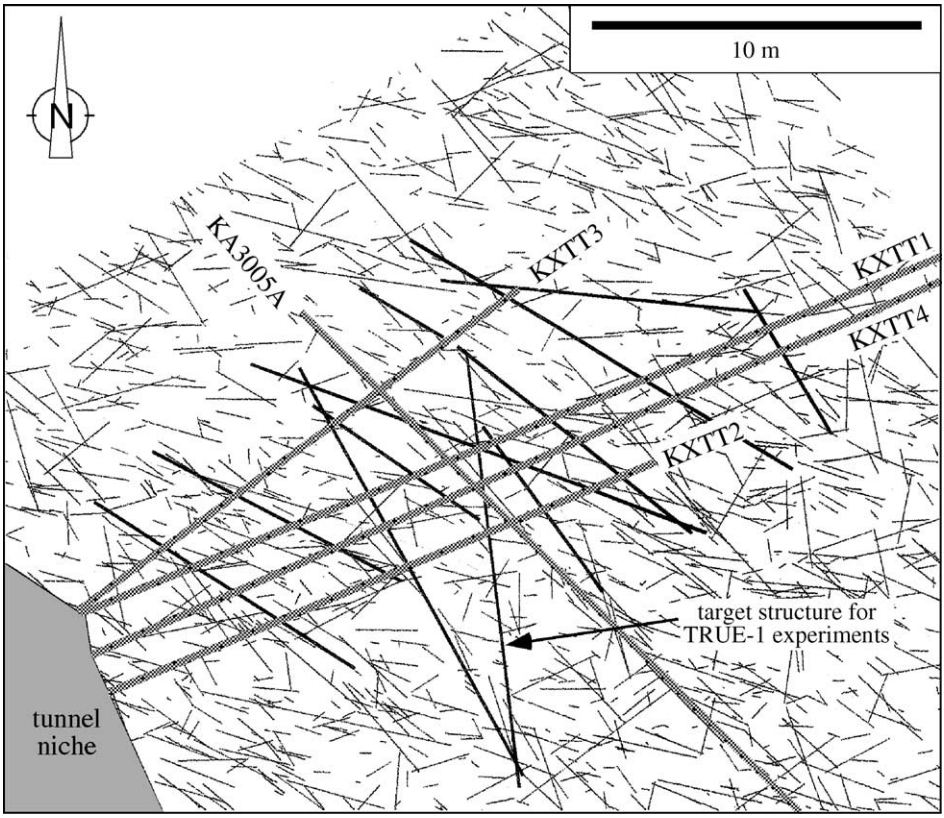

Fig. 3. Structural model of the TRUE-1 block in cross-section (plane dipping 40° towards ENE, i.e. parallel to the KXTT boreholes that are shown in grey). Thick lines represent mylonite zones containing interconnected networks of fractures.

is only weakly affected by mylonitic deformation, resulting in the development of a planar fabric (foliation). Very strong mylonitic deformation, producing fine-grained, mica-rich fabrics, is concentrated to a limited number of discrete horizons (typically three to six), each of which is only a few centimetres thick. These horizons focus the development of younger, brittle structures, such as cataclasites and open fractures, as illustrated in Fig. 4 (top part). Because of their enhanced connectivity on a scale of metres at least, a structure of this type has been chosen as the target for crosshole tracer testing (shown in Fig. 3) and will be dealt with below and in Jakob et al. (2003).

3.2. Structural model of the TRUE-1 block

A structural model of the TRUE-1 block was derived on the basis of geological and hydraulic information from the boreholes, core materials and from the adjacent tunnel wall and is shown in Fig. 3. In the immediate surroundings of the boreholes, deterministic information based on core and borehole logging was used. However, the larger part of the

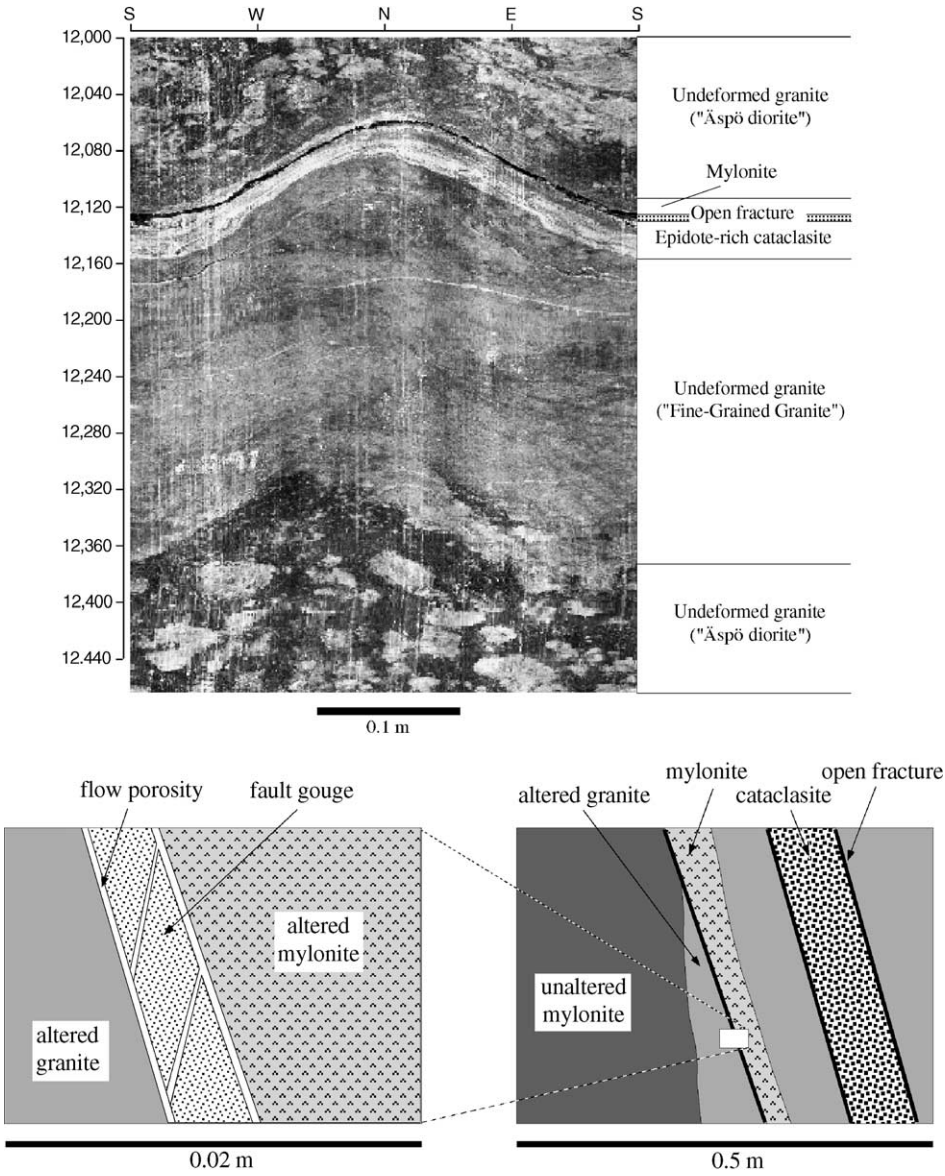

Fig. 4. Detailed-scale geometry of fractures within the TRUE-1 block. Top: borehole-wall image showing an example of the fractures subjected to crosshole testing (scale in metres along hole). Bottom: small-scale conceptual model.

model volume had to be described stochastically (based on discrete fracture network modelling) because individual fractures are mostly shorter than 1 m and cannot be extrapolated over larger distances away from their intersections with boreholes. The only

structures that can be correlated between different boreholes are extended fracture systems that follow mylonitic zones, and these are represented by thick lines in Fig. 3. The density of fractures in the model volume is very large. As the majority of all fractures is transmissive, it is concluded that the TRUE-1 block represents a hydraulically well-connected fracture network, with mylonitic zones representing the corridors of maximum fracture frequency and connectivity.

4. Detailed-scale geometry and conceptualisation of fractures in the TRUE-1 block

Fig. 4 (top part) shows a 360° borehole-wall image of one of the intercepts of the mylonite-hosted fracture that was subjected to crosshole tracer testing. While this structure belongs to a smaller size hierarchy when compared to the larger structure shown in Fig. 2, the anatomy of both structures is remarkably analogous, reflecting the same geological evolution with recurrent deformation/alteration events that result in the same types of fault rocks. The structure in Fig. 4 consists of a mylonitic zone that was recurrently reactivated by faulting. Thus, it contains cataclasite as well as uncemented, open fractures. The only difference is the fact that no fault gouge was observed. This can be due either to the absence of gouge in situ or to washing out of the friable gouges during the drilling process. From a geological point of view, it appears very likely that gouge materials are present in situ (even though probably less in quantity than on the larger scale) because of the analogy of the fault anatomies and deformation processes on both scales. Thus, the presence of gouge in the target structure for tracer testing is inferred by downscaling observations made on faults of a larger size hierarchy.

For the sake of understanding and quantifying tracer transport and retardation in the tracer tests that were conducted in the TRUE-1 volume, a detailed-scale geometric conceptual model of representative fractures was developed and is shown in Fig. 4 (bottom part). It integrates direct evidence from core and borehole logging, insights based on the understanding of the deformation mechanisms and information derived from larger-scale faults at Äspö.

Table 1
Average mineralogical compositions and matrix porosities of rock types occurring adjacent to open fractures

Data in wt.%	Fresh granite	Mylonite	Cataclasite	Fault gouge
Quartz	17	15	10	12
Plagioclase	44	30	14	7
K-feldspar	13	21	14	11
Biotite	13	23	+	0
Epidote	5	5	45	4
Chlorite	+	+	14	44
Fe-oxides	0	0	+	+
Calcite	+	+	+	4
Accessories	5	3	2	3
Clay minerals	0	0	+	12
Porosity (vol%)	0.3	0.05	0.5–3.0	10–30

"+" = occurrence in trace amounts.

Table 1 lists the mineralogical compositions and matrix porosities of all rock domains that are represented in the model. Porosity varies over orders of magnitude between different rock types, and the presence of clay minerals in fault gouge and in cataclasite suggests that sorption characteristics of these brittle fault rocks are most likely contrasting to those of the other rock types. It follows that fault gouge and, to a lesser degree, cataclasite are the rock types with high porosities and expected high sorption K_d values that dominate tracer retardation during the short-duration tracer tests.

5. Modelling framework

5.1. Rationale

A series of dipole tracer tests, using different radioactive tracers, was conducted in the reactivated mylonitic structure described above. In this paper and in Jakob et al. (2003), we focus on the first tracer test STT1 only, with a distance of ca. 5 m between the injection and extraction boreholes. For this test, tracer breakthroughs were predicted blindly, i.e. without knowledge of the actual experimental results. The main objective of the exercise was to test the adequacy of different models from various modelling teams (including the choice of processes to be considered) as well as of field- and laboratory-derived parameters. Input data that were provided to the modellers included:

- results from a previous dipole test (PDT3) in the same test interval, including the injection distribution function, test conditions and the uranine breakthrough data;
- the tracer injection function and the injection/extraction rates of the STT1 test;
- laboratory-derived measurements for the pore diffusion coefficients D_p and sorption K_d (mass-based) and K_a (surface-based) values for fresh granite. These sorption data were rescaled in order to be applicable for fracture-filling gouge materials. The rescaling, together with the numeric values for all parameters, is documented in Jakob et al. (2003).

In addition, a large amount of geological information was available to constrain the model geometry and detailed structure of the flowpath between injection and extraction (see above).

5.2. Geometry of the flow field and model calibration

Given the scale of the experiments (ca. 5 m), it was assumed that heterogeneities on the decimetre or even metre scale would play only a minor role. Due to the large hydraulic gradient of ca. 1.5–2 m/m that was used for the experiments, the expected width of the transport domain is very restricted. Calculations in the frame of the 2D-streamtube model with an underlying homogeneous and isotropic transmissivity field (also taking into account the influence of the background flow field with a gradient of 0.066 m/m towards the tunnel) indeed corroborated these expectations. Thus, in spite of the structural complexity shown in Fig. 3, the transport domain does not characterise the full fracture

network of the TRUE-1 block but is limited to a narrow pipe within the network (Fig. 5). By analysing the time-dependent uranine injection distribution in the PDT3 test, a value for the time-independent injection flow rate Q_i of 0.444 ml/min could be determined. For the calibration run PDT3 and the subsequent tracer test STT1, a fixed pumping rate Q_e of about 400 ml/min was used as the downstream boundary. The resulting ratio Q_e/Q_i of 900 also illustrates the monopole-like flow field and the narrow shape of the transport domain.

5.3. Role of matrix diffusion

Matrix diffusion is an important retarding and dispersing transport mechanism for solutes carried by groundwater in fractured porous media. It retards solutes by

1) spreading them from the flowing groundwater into the diluting reservoir of the interconnected pore space of the rock matrix, and
2) providing an increased surface for sorption processes.

Matrix diffusion has been studied either by small-scale laboratory (e.g. Hadermann, 1992; Bear et al., 1993) or larger-scale field tracer experiments (e.g. Heer and Hadermann, 1994; Hadermann and Heer, 1996; Meigs et al., 1997; Heer and Smith, 1998).

The uranine breakthrough of the PDT3 test (Fig. 6a) clearly reveals a relatively simple structure with a pronounced tailing. In a log–log representation, a $t^{-3/2}$ dependency could be observed, which is considered to be diagnostic for a marked effect of matrix diffusion. In addition, an additional hump on the trailing edge could be seen, which was interpreted as a possible spatial limitation (boundary) of the porous rock accessible to matrix diffusion.

In order to test the assumption that matrix diffusion has to be taken into account, an attempt was made to model the measured breakthrough curve with the help of a simple

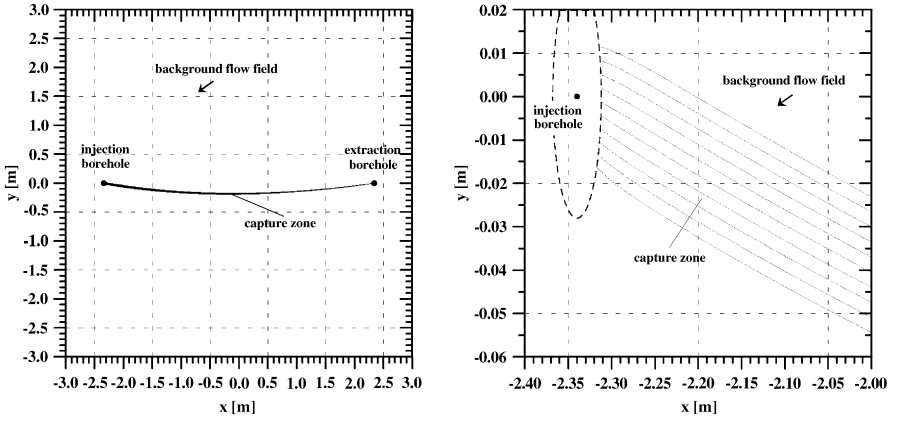

Fig. 5. Transport domain for the PDT3 and STT1 tracer tests represented by 10 streamlines (right part is a close-up in the vicinity of the injection borehole). The capture zone (transport domain) is very narrow and distorted due to a weak background flow field.

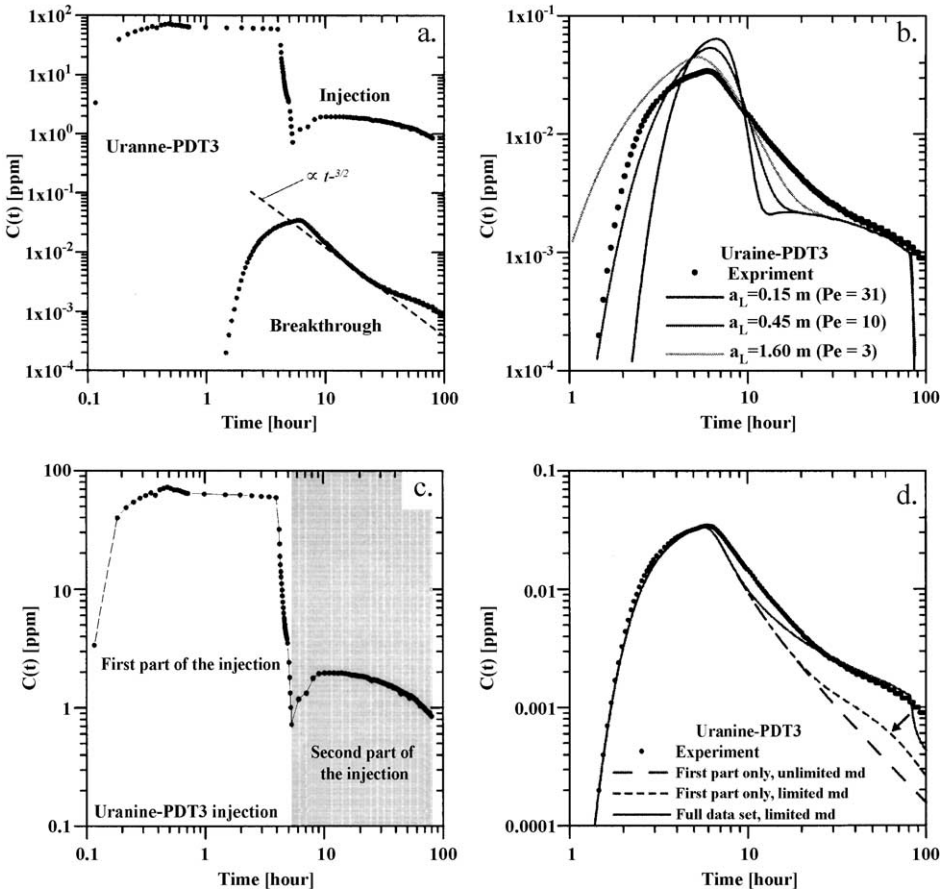

Fig. 6. Analysis of the PDT3 tracer test. (a) Measured uranine injection and breakthrough concentration versus time. The straight dashed line illustrates the $t^{-3/2}$ dependency of a part of the trailing edge of the breakthrough curve, which is indicative for matrix diffusion. (b) Influence of the longitudinal dispersion length a_L in the frame of the 1D-advection/dispersion model on uranine breakthrough. (c) Uranine release as a function of time. After about 5 1/2 h, a first tracer pulse is followed by a second, 35 times less pronounced pulse. (d) Series of calculated tracer breakthrough curves, where different parts of the injection function were considered. The strong decrease in the tail (solid line) for times larger than 80 h is caused by missing data of the second part of the injection distribution. ("md" = matrix diffusion).

1D-advection/dispersion model where the only freely adjustable parameters are the flow width (and hence the water velocity) and the Peclet number. The flow width roughly accounts for the peak arrival time, and the shape of the breakthrough curve is mainly influenced by (longitudinal) dispersion. The best-fit value for the flow width is 1.4 mm, which is equal to the fracture aperture of Andersson et al. (1997, Tables 1 and 2). Furthermore, a best-fit value for the longitudinal dispersion length a_L of 0.45 m could be determined. However, as shown in Fig. 6b, the shape of the breakthrough curve is only very roughly reproduced and the predicted peak maximum is 1.6 times too high,

irrespective of the choice of the value for the dispersion length. It is concluded that an advection/dispersion model alone cannot explain the measurements.

According to the geological conceptual model of the migration pathways in the TRUE-1 block (Fig. 4), brittle fault rocks occur adjacent to the fractures in which flow occurs, namely fault gouge and cataclasite. Specifically, the former has a very high porosity (Table 1) and is therefore of potential relevance for matrix diffusion. In contrast, rock types unaffected by brittle deformation (e.g. mylonite, granite) can be regarded as inaccessible over the time scales considered in the experiment (hours–days) because they have porosities that are orders of magnitude lower. Based on these considerations, a model calculation assuming limited matrix diffusion into a 1-mm thick fault gouge (value based on geological estimates of fault gouge thickness) turned out to provide a very good fit to the experimental data (Fig. 6d—full data set). Thus, both the shape of the uranine breakthrough curve in test PDT3 and independent geological information indicate that matrix diffusion into fault rocks needs to be considered for modelling purposes. In contrast, advective water flow in the fault rocks is most likely negligible due to the very small pore apertures and therefore low permeabilities.

According to geological information, matrix diffusion is expected to reach a physical boundary, eventually resulting in saturation (i.e. similar solute concentrations in the fracture and in the porous matrix). Once the concentrations in the fracture decline, this will result in an increased solute backflow, followed by a rapid drop once the reservoir is drained. In the breakthrough curve, such a boundary effect is recognised by a second hump (the so-called tail end perturbation) that modifies the $t^{-3/2}$ slope of the trailing edge. Unfortunately, due to the shape of the experimental injection function, the analysis of the uranine breakthrough curve of PDT3 was inconclusive with respect to such boundary effects. A second prominent tracer-injection pulse after about 5 1/2 h (Fig. 6c) masked a possible tail end perturbation completely, although the tracer release was a factor of 35 smaller than the main tracer injection. In the right part of Fig. 6d, the solid line represents the calculated breakthrough using the full dataset concerning uranine injection, and the dashed lines only consider the tracer release up to 5 1/2 h. It can be seen that the second injection signal has a substantial effect on the shape of the breakthrough curve, making the recognition of physical boundary effects of the porous material impossible.

6. Extrapolation to larger scales in time and space

6.1. Fracture geometries on different scales

As shown in Fig. 7 (after Bossart et al., 2001), fractures and faults at Äspö occur on a wide range of scales. The following hierarchies can be distinguished:

1) Small-scale fracture network (e.g. the background fracturing within the TRUE-1 block, fracture size in the range of decimetres to a few metres, Fig. 7d);
2) Zones of enhanced fracture frequency and connectivity within the small-scale fracture network, typically along ductile precursors (Fig. 7a–d);
3) Network of decametre-size faults (Figs. 1 and 7e);

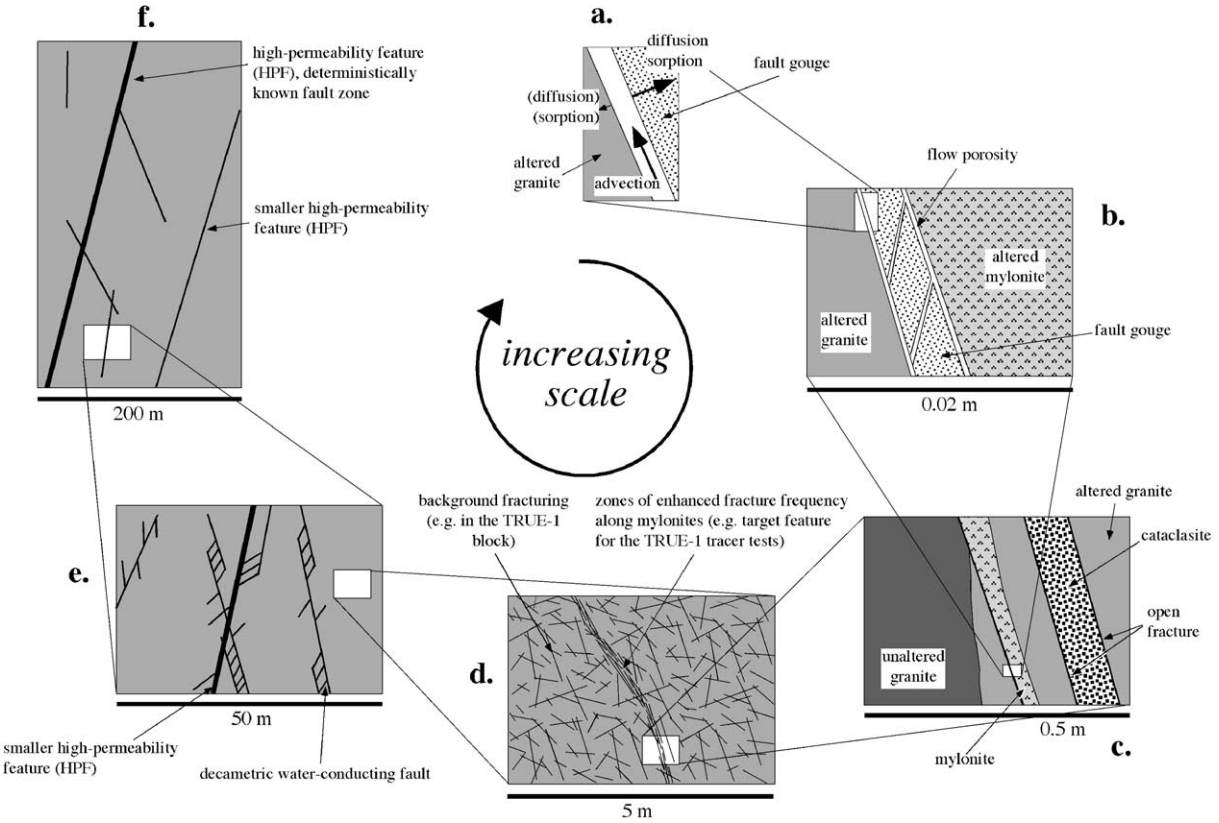

Fig. 7. Series of conceptual models showing fracture geometries and water flowpaths on a range of scales.

4) High-permeability features (HPFs according to Rhén and Forsmark, 2000), including deterministically known regional faults and lineaments (Fig. 7e and f).

When considering contaminant transport through the geosphere, both the spatial and temporal scales are much larger than those of the in situ experiments. Assuming a leaking contaminant source away from major water-conducting features, i.e. with a certain "respect distance" to the nearest conductors, transport will occur through all the fracture-size hierarchies given above before possible exfiltration at the surface. Contaminants would be first transported through low-permeability fractures of limited size. Due to the good interconnection of fracture systems on all scales, they would eventually exfiltrate into larger-scale and higher-permeability networks and finally into high-permeability features (major faults and lineaments).

In geosphere transport calculations, the contribution of the first section of the release path to contaminant retardation typically dominates over the contribution of the downstream flowpaths through higher hierarchies of fractures (e.g. Nagra, 1994). This is in part due to the higher permeability in the larger structures, but also due to the more limited ability of full hydrogeological characterisation of the large structures (and therefore the need for conservative assumptions that minimise retardation). Thus, the characterisation of the size and the properties of the first part of the release path is of crucial importance. Because the TRUE-1 tracer experiments were performed in relatively small structures, they can only be used to constrain the early parts of the release paths of contaminants.

6.2. The effect of transport time

The time scale of the TRUE-1 dipole experiments is hours to days, which explains why tracer/rock interactions, such as matrix diffusion and sorption, occur only on the fracture walls and the adjacent few millimetres of rock. If longer time scales for transport are considered, the penetration depth of matrix diffusion will be substantially larger (proportional to the square root of time) and thus, interactions will not only occur with the thin fault rocks (such as fault gouge and cataclasite) but also with adjacent undeformed granite. Because the latter has a much smaller porosity, matrix diffusion will be less efficient. In addition, there are mineralogical distinctions between the fault rocks (which often contain clay minerals) and the granite (see Table 1), which means that sorption in granite will be less pronounced. K_d values of granite can be more than one order of magnitude smaller than those of a clay-containing fault gouge. The combined effects of slower matrix diffusion and more limited sorption are expected to result in a less efficient retardation when compared to the short-duration experiments. It is concluded that, provided an interconnected porosity exists in undeformed granite, tracer retardation will occur even over large scales in time and space, but its magnitude is expected to be smaller.

7. Conclusions

The granitic rocks at Äspö contain water-conducting features on a wide range of scales, from regional (kilometric) lineaments to decimetric fractures. Water-conducting features on

a scale of decametres and more are related to steeply dipping faults and contain a variety of fault rocks, including mylonites, cataclasites and fault gouges. Smaller-scale fracture patterns were studied in the TRUE-1 block, which is bounded by the decametric faults. It contains a network of fractures with sizes in the range of decimetres to metres that are interconnected in three dimensions. Ductile precursors (mylonites) act as focus for enhanced fracture frequency and thus, constitute well-interconnected and more highly conductive corridors in the rock volume considered. One of these was the target of the dipole tracer experiments. The application of the geological studies to tracer-transport calculations resulted in the following conclusions:

- In spite of the large number of investigation methods applied and the high data density, a fully deterministic model of the TRUE-1 block could not be derived due to substantial small-scale heterogeneity. The gaps were filled by conceptual considerations (e.g. enhanced fracturing in extended mylonitic zones) and by stochastic information (background fracturing).
- Matrix diffusion was identified as a process that occurs even over the short time scales of the experiments. Even though subordinate by volume, fault gouge is the most likely rock type in which diffusion may occur (high porosity, situated next to open fractures). However, advection through the very small pores in fault gouge is regarded as irrelevant.
- Rock types unaffected by brittle deformation, such as mylonite or granite, do not interact noticeably with the tracers, even though they account for the largest part of the rock volume.
- Due to the very high pumping rates, the experimental flow field is extremely narrow. Thus, whether flow and transport occur through one single structure or through a network of fractures, it will be largely one-dimensional and use the most efficient flowpath. Flow and transport under natural conditions will take place at much smaller hydraulic gradients and thus will spread more efficiently over the network.
- The irregular shape of the tracer injection distribution masked important information on the rock/nuclide interaction in the trailing edge of a breakthrough curve. Hence, for future tracer experiments, the techniques of tracer injection have to be improved. In addition, it would be highly beneficial to measure the trailing edge of a breakthrough curve down to very low values and longer times in order to record the effects of a possible tail end perturbation and thereby further constrain the models parameter space.
- The application of the TRUE-1 experiments to transport in larger scales in space and time is not straightforward and requires a good geometric understanding of water-conducting features on all scales in question. Over long time scales, matrix diffusion will penetrate the rock matrix beyond the fault gouges (which become saturated and therefore less significant). This requires new sets of relevant parameters, such as porosity, diffusion and sorption coefficients.

Acknowledgements

The authors would like to thank Peter Wikberg (SKB) for initiating the Fracture Characterisation and Classification Project as well as Jan Hermanson (Golder Associates, Sweden) and Anders Winberg (Conterra AB, Sweden) for their technical input at various

stages. Financial support by SKB (Sweden), Nagra (Switzerland) and PSI (Switzerland) is gratefully acknowledged. SKB staff at Äspö (headed by O. Olsson) readily provided local support when needed. Comments by two anonymous reviewers, U. Mäder, A. Matter and Tj. Peters (all Bern) improved the manuscript.

References

Andersson, P., Nordqvist, R., Jönsson, S., 1997. TRUE-1st Stage tracer test programme—experimental data and preliminary evaluation of the TRUE-1 dipole tracer tests DP-1–DP-4. SKB Progress Report HRL-97-13, SKB, Stockholm, Sweden.

Bear, J., Tsang, T.F., de Marsily, G. (Eds.), 1993. Flow and Contaminant Transport in Fractured Rock. Academic Press, San Diego.

Bossart, P., Hermanson, J., Mazurek, M., 2001. Analysis of fracture networks based on the integration of structural and hydrogeological observations on different scales. SKB Technical Report 01-21, SKB, Stockholm, Sweden.

Elert, M., Svensson, H., 2001. Evaluation of modelling of the TRUE-1 radially converging tests with sorbing tracers. The Äspö Task Force on Modelling of Groundwater Flow and Transport of Solutes, Tasks 4E and 4F. SKB Technical Report TR-01-12, SKB, Stockholm, Sweden.

Hadermann, J. (Ed.), 1992. The International INTRAVAL Project, Phase 1, Case 1bUranium Migration in Crystalline Rock; Borecore Pressure Infiltration Experiments. OECD/NEA, Paris, France.

Hadermann, J., Heer, W., 1996. The Grimsel (Switzerland) migration experiment: integrating field experiments, laboratory investigations and modelling. J. Contam. Hydrol. 21, 87–100.

Heer, W., Hadermann, J., 1994. Modelling radionuclide migration field experiments. PSI Report 94-13, Paul Scherrer Institute, Würenlingen and Villigen, Switzerland, and Nagra Technical Report NTB 94-18, Nagra, Wettingen, Switzerland.

Heer, W., Smith, P.A., 1998. Modelling the radionuclide migration experiments at Grimsel. What have we learnt? Mater. Res. Soc. Symp. Proc. 506, 663–670.

Jakob, A., Mazurek, M., Heer, W., 2003. Solute transport in crystalline rocks at Äspö: II. Blind-predictions, inverse modelling and lessons learnt from test STT1. J. Contam. Hydrol. 61, 175–190

Martel, S.J., Pollard, D.D., 1989. Mechanics of slip and fracture along small faults and simple strike-slip fault zones in granitic rock. J. Geophys. Res. 94, 9417–9428.

Mazurek, M., Bossart, P., Eliasson, T., 1996. Classification and characterisation of water-conducting features at Äspö: results of investigations on the outcrop scale. SKB International Cooperation Report ICR 97-01, SKB, Stockholm, Sweden.

Meigs, L.C., Beauheim, R.L., McCord, J.T., Tsang, Y.W., Haggerty, R., 1997. Design, modelling, and current interpretations of the H-19 and H-11 tracer tests at the WIPP site. Field Tracer Experiments: Role in the Prediction of Radionuclide Migration. Proceedings of GEOTRAP Workshop (Cologne, Germany, 28–30 August 1996) OECD/NEA, Paris, France, pp. 157–170.

Nagra, 1994. Kristallin-I—Safety assessment report. Nagra Technical Report NTB 93-22, Nagra, Wettingen, Switzerland.

Rhén, I., Forsmark, T., 2000. Äspö Hard Rock Laboratory—High-permeability features (HPF). SKB International Progress Report IPR 00-02, SKB, Stockholm, Sweden.

Stanfors, R., Erlström, M., Markström, I., 1997. Äspö HRL—Geoscientific evaluation 1997 1. Overview of site characterisation 1986–1995. SKB Technical Report TR 97-02, SKB, Stockholm, Sweden.

Stanfors, R., Rhén, I., Tullborg, E.L., Wikberg, P., 1999. Overview of geological and hydrogeological conditions of the Äspö hard rock laboratory site. Appl. Geochem. 14, 819–834.

Winberg, A. (Ed.), 1996. First TRUE Stage—Tracer Retention Understanding Experiments: descriptive structural–hydraulic models on block and detailed scales of the TRUE-1 site. SKB International Cooperation Report ICR 96-04, SKB, Stockholm, Sweden.

Winberg, A., Andersson, P., Hermanson, J., Byegård, J., Cvetkovic, V., Birgersson, L., 2000. Äspö Hard Rock Laboratory—final report of the first stage of the tracer retention understanding experiments. SKB Technical Report TR 00-07, SKB, Stockholm, Sweden.